12-2020

Sequential damage study induced in fiber reinforced composites by shear and tensile stress using a newly developed Arcan fixture

Israr Ud Din

Shanshan Tu

Pei Hao

Stéphane Panier

Kamran Ahmed Khan

See next page for additional authors

10.1016/j.jmrt.2020.09.067

Din, I. U., Tu, S., Hao, P., Panier, S., Khan, K. A., Umer, R., ... Aamir, M. (2020). Sequential damage study induced in fiber reinforced composites by shear and tensile stress using a newly developed Arcan fixture. *Journal of Materials Research and Technology, 9*(6), 13352-13364. https://doi.org/10.1016/j.jmrt.2020.09.067

Available online at www.sciencedirect.com

jmr&t Journal of Materials Research and Technology

https://www.journals.elsevier.com/journal-of-materials-research-and-technology

Original Article

Sequential damage study induced in fiber reinforced composites by shear and tensile stress using a newly developed Arcan fixture

Israr Ud Din[a], *Shanshan Tu*[b,*], *Pei Hao*[c], *Stéphane Panier*[c], *Kamran Ahmed Khan*[d], *Rehan Umer*[d], *S.Z.H. Shah*[e], *Gérald Franz*[c], *Muhammad Aamir*[f]

[a] *Research Centre for Modelling & Simulation (RCMS), National University of Sciences and Technology (NUST), Sector H-12, Islamabad, Pakistan*

[b] *Research Center of Intelligent Perception and Autonomous Control, Faculty of Information Technology, Beijing University of Technology, Beijing, 100124, PR China*

[c] *Laboratoire des Technologies Innovantes, LTI-EA 3899, Université de Picardie Jules Verne, Amiens, 80025 France*

[d] *Department of Aerospace Engineering, Khalifa University of Science and Technology, Abu Dhabi, United Arab Emirates*

[e] *Department of Mechanical Engineering, Universiti Teknologi PETRONAS, 32610 Bandar Seri Iskandar, Perak, Malaysia*

[f] *School of Engineering, Edith Cowan University, Joondalup, WA 6027, Australia*

ARTICLE INFO

Article history:
Received 26 July 2020
Accepted 12 September 2020

Keywords:
Modified Arcan fixture
Sequential damage
In-Plane loading
Numerical analysis
Fiber reinforced polymers

ABSTRACT

This work presents the application of both uniaxial and bi-axial in-plane loads to unidirectional carbon fiber reinforced polymer laminates using a newly developed Arcan fixture, which is a reliable experimental set-up to obtain a uniform shear stress field in a butterfly specimen. The set-up can be used for both damage model validation and parameters identification at various fiber orientations while using the same specimens. A sequential damage study was completed to highlight the influence of diffused damage induced in pure shear on the fiber direction tensile behavior of the laminate. This was accomplished by applying load on the specimens in two steps: (i) the pure shear step and then unloading at approximately 70% of the shear failure strength, (ii) in the tensile step until final failure. A clear drop in the tensile behavior of the laminate was observed by the diffused damage induced in the first loading step of pure shear. The experimental study is also supplemented with numerical simulations using a nonlinear elasto-plastic coupled damage constitutive law by employing Puck's failure theory for mesodamage activation. In addition to the damage pattern, the non-linear mechanical behavior in shear is predicted and found in good correspondence with the experimental results.

* *Corresponding author.*
E-mails: israr.rcms@rcms.nust.edu.pk (I. Ud Din), sstu@bjut.edu.cn (S. Tu), pei.hai@u-picardie.fr (P. Hao), stephane.panier@u-picardie.fr (S. Panier), kamran.khan@ku.ac.ae (K.A. Khan), Rehan.umer@ku.ac.ae (R. Umer), syed_17005802@utp.edu.my (S. Shah), gerald.franz@u-picardie.fr (G. Franz), m.aamir@ecu.edu.au (M. Aamir).

https://doi.org/10.1016/j.jmrt.2020.09.067

1. Introduction

High performance fiber reinforced polymers (FRPs) are considered as one of the most important composite materials used in the structural applications of various industries such as aerospace, marine, automotive and sports industry [1–3]. Material characterization is a pre-requisite to predict the structural response of composite materials with the assistance of numerical simulations in the product development phase. Due to anisotropy in case of composite materials, these properties need to be determined in various principal material directions according to designated standards. Olsson [4] has highlighted that the strength and failure characteristics of FRPs under the combined effect of in-plane shear and tensile normal stresses are deemed highly important for the effective serviceability of composite structures. The mechanical performance of composite materials against shear stress further decreases in the presence of both tensile stress and shear stress. This deterioration is obvious in the failure envelope in the first quadrant of shear and normal stress in advanced failure theories such as Puck's theory [5] and Cuntze's theory [6]. Puck's theory has been used in the contact problem by Ud Din et al. [7], where it has been demonstrated that stress interaction is highly influential on the mechanical behavior of composite materials.

There are several methods for in-plane shear testing of composite materials. The most common method is testing of $\pm 45^{\circ}$ symmetric laminate about the mid-plane in tensile loading. In such test, the transverse strain ε_{22} is very small and shear strain ε_{12} is about thirteen times that of the fiber direction strain ε_{11} [4,8]. The next method is the application of tensile loading on the laminate having fiber oriented at an angle of about 10°. In this case, the transverse normal strain ε_{22} is almost zero and shear strain ε_{12} is about 3–4 times the strain of the fiber direction ε_{11}. There are inherent difficulties encountered in this testing such as the use of loading clamps and the requirement of longer specimens which result in bending. Paepegem et al. [8] have obtained considerably lower strength using the 10° fiber orientation sample compared to the $\pm 45^{\circ}$ symmetric laminate. In addition to these configurations, other experimental methods for in-plane shear characterization include a V-notch rail shear test (ASTM D7078-12), and V-notch beam test method, which is also known as Iosipescu shear test (ASTM D5379-12) as mentioned by Tan et al. [9] for carbon fiber reinforced polymers (CFRPs), and by Khashaba [10] for in-plane loading at angles ranging from 0° to 90°. However, these configurations need specialized test fixtures in contrast to the laminates of $\pm 45^{\circ}$ and 10°. Likewise, inter-laminar shear strength (ILSS) is also determined by two tests including the short beams test (ASTM D2344-13) and the double V-notch test where the details of these characterizations tests are given in [11].

The in-plane tensile test of $\pm 45^{\circ}$ laminate for FRPs has been widely adopted in accordance with ASTM D3518/D3518 M (the equivalent in ISO 14129:1997) because of its easier method for characterizing the shear performance of the material. Accordingly, the laminate is loaded along the global 0° direction and the stress is taken as half of the longitudinal stress as recorded in the experiment based on the stress transformation to the maximum shear stress plane. Nevertheless, normal stresses in the fiber direction and transverse to the fiber direction also exist in this test, thus affecting the results by stress-interaction [12]. Olsson [4] has also compared available testing methods for shear characterization of composites in which attention was given to both merits and demerits of tubular specimens, cruciform specimens, and Arcan specimens. The advantage of tubular specimens is their absence of free-edge-effect, which covers most of the failure envelope quadrants. However, the fabrication of the tube and its control in manufacturing quality in addition to performing experiments is a challenging task [13]. On the other hand, cruciform specimens can be employed for in-plane bi-axial normal stresses and are comparatively easier to fabricate. However, the testing rig requires four orthogonal loading actuators. The Arcan specimen can only be used for in-plane shear with tension or compression, where in cases of compression a fairly complex supporting rig is required [4]. Shear testing with Arcan of AS4/PEEK in [14] has indicated a higher strength than the conventional off-axis test of $\pm 45^{\circ}$ compliant with ASTM D3518/D3518 M. Therefore, shear characterization of FRPs based on the Arcan fixture is considered as one of the important methods to measure realistic shear strength and exploit composites to their best capabilities. Besides, the in-plane application of loading on various types of composites, Arcan fixture has also been used in many studies for out-of-plane quasi-static testing as well as for delamination [15–17]. Based on review of available literature, the Arcan fixture has been less studied in fatigue loading compared to bi-axial fatigue studies using cruciform specimens as investigated in [18,19]. Therefore, the Arcan fixture presents a potential for exerting bi-axial fatigue loading of tensile stress in combination with shear stress as reported in [20].

Nouri et al. [21] completed an experimental study limited to intra-laminar damage mechanisms to evaluate the effects of diffused damage induced in shear loading on transverse meso-cracking in uni-directional (UD) CFRPs. The study showed that diffused damage acts as a foundation for transverse cracking in a single ply. Furthermore, transverse cracks are the mesoscopic cracks that develop along with the whole thickness of a single lamina [22]. In principle, shear stresses in FRPs invoke these types of intra-laminar diffused damage and are responsible for the reduction of shear stiffness. The experimental procedure proposed by Nouri et al. [21] consisted of two steps of loading. Firstly, diffused damage was induced in $[\pm 45^{\circ}]_{2s}$ by applying tensile load on the composite coupon, then smaller samples were cut at 45° from the same tested coupon containing diffused/micro damages. In the second step of loading, the transverse cracking was initiated by exerting a tensile load on the smaller pre-damaged specimens at $[0/90_2/0]$ with stacking obtained in the first load step using Deben with a 5 kN load cell. Unlike the work presented by Nouri et al. [21], the present study utilizes the same pre-damaged specimen by rotating it at a particular angle to apply the tensile load. The testing of the same specimen avoids the machining of smaller specimens that may also contribute to damage during the machining. Accordingly, the conventional universal testing machine can be used for testing with no further equipment required.

Table 1 – CFRP constituents' material specifications.

Properties	
Fiber manufacturer	SAERTEX GmbH.
Fiber type	T700SC 50C
Carbon fiber density (g/cm^3)	1.79
Aerial density of carbon reinforcement (g/m^2)	154 ± 5.0
Filament diameter	7.0 microns
Polymer type and supplier	Sicomin SAS.
Thermoset polymer	Epoxy: SR 8100 Hardener: SD 8824
Laminate	
Theoretical desired fiber volume fraction (V_f)	55%
Dry thickness per ply (mm)	0.086
Wet thickness per ply (mm)	0.156

The present experimental set-up is robust and can be used at different angles to evaluate diffused damage in shear in combination with transverse stress components at various load ratios. In addition, this experimental set-up can be used in fatigue testing to evaluate the effect of diffused damage on transverse cracking. Therefore, in this study, a modified Arcan test fixture was used for in-plane shear stress alone as well as in combination with transverse tensile loading. The butterfly specimen compatible with the new Arcan fixture was modified, keeping in mind the objective to produce a uniform state of stress field greater than the sizes of the strain gauges in the notch section. This enabled us to acquire a uniform state of shear stress. The resin infusion technique was employed to fabricate the specimens for UD characterization and butterfly specimens. The mechanical properties, as a result of UD testing, were provided to the numerical simulations. Furthermore, the effects of diffused damage induced in the pure shear state of stress on the tensile behavior are discussed. For this purpose, the damage was first induced in the butterfly specimen by applying a pure shear load-step. Afterwards, the damaged specimen was rotated and the tensile mechanical behavior was studied. Strain gauges and digital image correlation (DIC) were utilized for strain field acquisition. Apart from the experimental work, non-linear damage coupled elasto-plastic constitutive law was used for numerical analysis in ABAQUS via user material subroutine (UMAT) in the implicit environment.

2. Materials and methods

2.1. *Material specifications and UD characterization*

The laminates used in this work were composed of UD carbon fibers and epoxy, as summarized in Table 1. A carbon fiber based UD dry fabric of 1.8 m width was procured with in-plane polyester stitching only for the sake of consolidation of the dry fabric and ease of handling. The aerial density for carbon fiber reinforcement and polyester yarn was 154 g/m^2 and 4 g/m^2, respectively. The dry fabric and stitching are shown in Fig. 1-a.

The required composite plates for fiber direction $[0^\circ]_6$, transverse direction $[90^\circ]_{12}$, and in shear $[\pm 45^\circ]_{2s}$ were fabricated with the resin-infusion method in the desired direction of the fiber orientation, as shown in Fig. 1-b. SR 8100 epoxy and SD 8824 hardener (mixing mass ratio: 100:33), which produce a low viscosity specialized system for the infusion process, was injected into the dry layers in the vacuum bag at approximately -0.9 bar pressure differential. The required fiber volume fraction (V_f) was 55%. The wet ply thickness was calculated based on the desired fiber volume fraction of 0.156 mm. Therefore, six plies were laminated to obtain a plate for the tension test in the fiber direction. The V_f was then recalculated and found as 52%. The final fabricated panel of $[0^\circ]_6$ laminate with a nominal thickness of 1 mm for the fiber direction tension test, is depicted in Fig. 1-c. As per manufacturer instructions, all fabricated plates were de-molded after 24 h and were cured for 8 h maintained at 60 °C in a programmable curing oven BINDER®.

The composite coupons as per the applicable ASTM standard for each type of characterization test were machined from the panels. Flat rectangular specimens were cut with precaution to avoid any damage for all tests, with the help of cutting wheel machine SSCM 800 MATRIX. During the cutting process, water was used as a coolant to prevent heating, the associated thermal deformation and the residual stress. Furthermore, rectangular tabs of 2 mm thickness were cut from aluminum alloy panels and were bonded at the ends of all the specimens to transfer the load smoothly, reduce stress concentration, and strengthen gripping in the testing machine, as well as to prevent any slippage. Scotch-Weld structural adhesive with trade name DP 490™ was used for gluing the tabs. Finally, the specimens were passed through 24 h curing cycle at ambient temperature to ensure secure bonding of the aluminum tabs with the composite surfaces.

A LLOYD LR50 K PLUS tensile machine with a load cell capacity of 50 kN was used in mechanical testing with the crosshead speed set at 1 mm/min for tests in the fiber direction, and 2 mm/min for tests in off-axis direction. All tests were conducted in displacement-controlled mode at room temperature. For strain measurement, an Epsilon™ extensometer was used with a gauge length of 25 mm in case of fiber direction testing and transverse direction testing. In the case of shear characterization, digital image correlation (DIC) was utilized to record the complete strain fields.

2.2. *Arcan fixture and butterfly specimen*

For shear characterization, the original Arcan fixture was modified by Yen et al. [23] which was also later used by El-Hajjar et al. [14]. The specimen is tightly clamped in four steel parts and its orientation is fixed in reference to these halves. The Arcan fixture is mounted in the loading machine with the help of clevis pins. The Arcan fixture used in [14,24] was modified by the authors of the present work to improve the performance and ease in manufacturing [25,26]. The butterfly specimen compatible with the dimensions of the new fixture is shown in Fig. 2-a [25]. The notch radius denoted by r is 2.38 mm and the angle α is 102.7°. D and W are the total length and width of the Arcan specimen. Besides, h and L describe the size of the uniform shear stress field. The CAD model of the modified Arcan fixture is depicted in Fig. 2-b-d, at different loading angles [25]. It should be noted that the specimen position is in the middle to avoid any eccentricity of the applied load, where

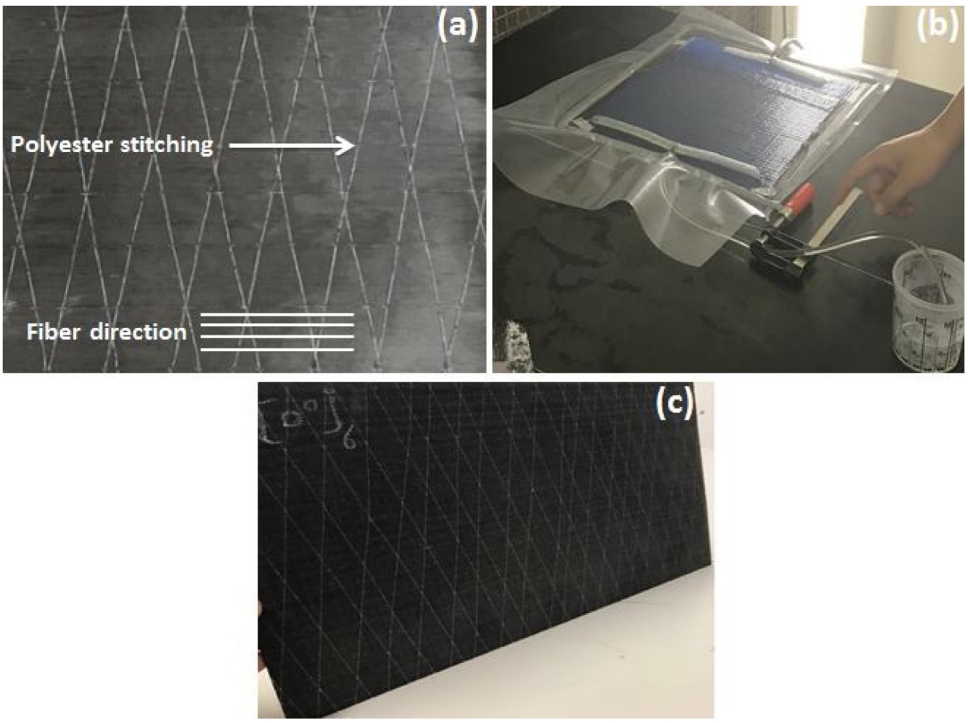

Fig. 1 – (a) Carbon fiber dry fabric and polyester (PES) stitching, (b) resin-infusion process, (c) cured UD plate.

θ denotes the angle between the applied load P and the notch section.

Two different laminates were planned for testing of Arcan butterfly specimens. In the first laminate, the fibers run perpendicular to the notch section denoted as $[90^\circ]_{16}$ whereas the second laminate is a cross-ply laminate i.e. $[0/90^\circ]_{4s}$. Gning et al. [17] have also conducted bi-axial testing on $[0/90^\circ]_{4s}$ using the classical Arcan fixture. These two categories of Arcan specimens are used for pure shear stress-strain behavior and will be compared with shear stress-strain curve obtained in the tension test of $[\pm 45^\circ]_{2s}$ in addition to bi-axial loading. The butterfly specimens were cut from plates with a precise tolerance water-jet cutting machine. The edges of all the Arcan specimens were inspected to detect any damage. Woven glass fiber tabs of same ends' profile as of Arcan butterfly specimens were used for firm gripping. Five Arcan samples with strain gauges installed for two configurations of $[90^\circ]_{16}$ and $[0/90^\circ]_{4s}$ each are shown in Fig. 3.

Two strain gauges having size of 6 mm gauge length, and 10 mm total length including soldering legs were glued along the x-axis, and y-axis with tolerance in resistance of $\pm 0.50\ \Omega$, and maximum resistance capacity of 118.6 Ω, as supplied by the Tokyo Measuring Instrument Lab (TML Co.). A gauge factor of 2.13 was used for the conversion of relative resistivity into the strain. The zone of uniform shear in the Arcan specimen in this study was 10 mm as denoted by h in Fig. 2-a. Therefore, the size of the pure shear zone is adequate for the strain gauges to be mounted. In addition to the strain gauges, an Allied® CMOS (Complementary Metal-Oxide-Semiconductor) camera with a resolution of 2048 horizontal pixels × 2048 vertical pixels was utilized to capture images of the deformed specimen surface. A frequency of four images per second (0.25 s/pic) was used during the experiments. The digital image correlation (DIC) method was implemented to measure the strain fields with Vic-2D® commercial software based on the captured images.

2.3. *Constitutive modeling*

Modeling of damage in FRPs is a complex task keeping in view the heterogeneous nature of composite materials in addition to the multi-scale nature of the damage development and progression. There are three scales for the development of the damage models which include microscale, mesoscale, and macroscale. The selection of a unit cell or representative volume element (RVE) for microscale and mesoscale depends on the type and architectural topology of reinforcement in composite material. For instance, if a laminate is embedded with only UD plies then the ply-level is considered as the meso-scale in case of UD fiber reinforcement, and a single homogenized ply is treated as a unit cell having material principal planes. These models are also known as ply-level models such as the elementary ply level model of Ladevèze et al. [27]. Besides, there are various other meso-scale models available for UD FRPs, few of them can be found in [28–33]. Indeed, the ply-level damage modeling results the model as a stacking-independent model which imparts versatility to the model with respect to the stacking sequence. As far as the microscale damage models are concerned, the unit cell for model based on this scale consists of constituents' properties to be provided as inputs in addition to the interface properties. Each constituent and their interface follow its own constitutive law [34–36].

The aforementioned subscale models represent the microstructural details with great accuracy. However, it is not

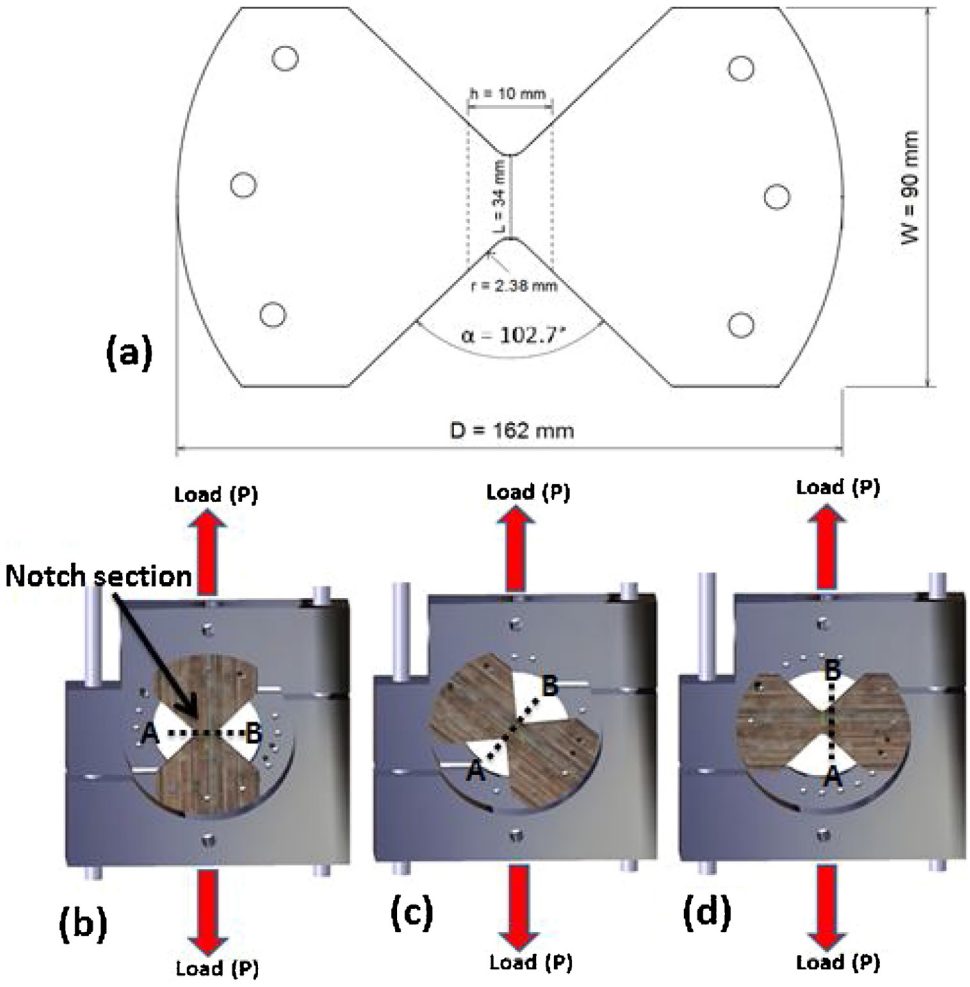

Fig. 2 – (a) Sketch of the butterfly specimen, (b) tension load, P ($\theta^0 = 90^0$), (c) combined load, P ($0 < \theta^0 < 90^0$) (d) pure shear load, P ($\theta^0 = 0^0$) [25].

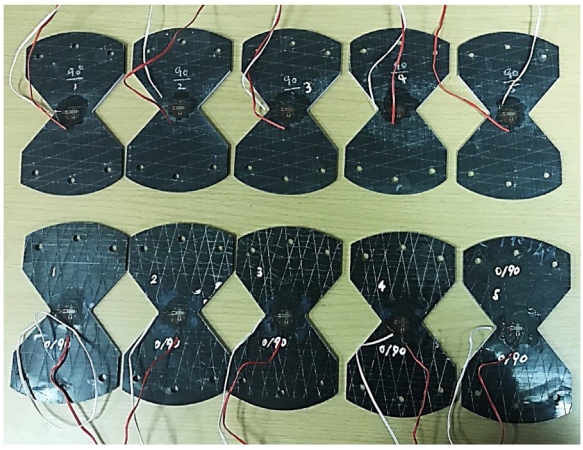

Fig. 3 – Arcan specimens: $[90°]_{16}$ and $[0/90°]_{4s}$.

always possible to employ such complicated models in the industrial environment for large scale composite structures due to the requirement of modeling each layer in a laminate, and need of finer mesh. As finer mesh is normally required in the ply-level energy based smeared crack damage models which are computationally expensive in case of large structures. Hence, computational models for the FE analysis of composites shall be developed keeping in consideration the requirements of industrial sectors [37]. To address these issues, laminate level models are developed with the motivation to be used in the industrial applications by reducing the computation and modeling effort where layered shell elements are used for sublaminate repetitive cell. Therefore, each element represents a sublaminate enabling the FE simulation of real size structures [38,39]. Most of the models incorporate either elasto-plasticity coupling with damage [29,33] or viscoelasticity-viscoplasticity [30]. In contrast to the previous modeling approaches, more recently, a group of investigators have developed a series of multiphase constitutive models that are capable of capturing the very complicated elasto-thermo-visco-plasticity and damage behavior of composite materials in a universal sense by properly addressing the coupling effects of strain rate, stress state, temperature and history dependency on their thermo-mechanical responses [40–43].

Based on our previous work and following the concept of continuum damage mechanics (CDM) as referred to in [27,44,45], a damage/plasticity coupled model was developed for the mesoscale of UD FRPs [22]. In CDM, the physical damage mechanisms are smeared out over the continuum and a degraded medium is modeled having lower load carrying capability than the virgin material. Once the damage is initiated based on any failure theory, then the damage is accumulated using the failure index as a function of fracture energies, elastic constants, and strength parameters of the ply in a laminate. For the purpose of completeness, the model developed by Ud Din et al. [22] is briefly discussed here.

The effective stress vector is denoted by $\tilde{\sigma}$ which can be mapped as a function of the actual Cauchy stress vector (σ_{22}) with the help of damage effect tensor $M(d)$ as:

$$\tilde{\sigma} = M(d) \,.\, \sigma \tag{1}$$

The damage effect tensor $M(d)$ which is the function of the damage variables is given as:$M\,(d) = diag\left[\frac{1}{1-d_1}; \frac{1}{1-d_2}; \frac{1}{1-d_{21}}\right]$

Here d_1, d_2 describe the damage variables in the material principal axis and $d_{21}$is the in-plane shear damage variable. All the damage variables are monotonically increasing due to the irreversibility of the damage i.e. no healing effects of the damaged material. 2D Puck's theory [5] given by Eq. (2) has been used for the onset of intra-ply mesoscale damage by treating individual ply as a homogenized continuum. For the description of each parameter in Eq. (2) readers are referred to [5,22].

$$\begin{aligned}
f_{E,FF,T} &= \frac{1}{X_T}\left[\tilde{\sigma}_{11} - \left(\upsilon_{21} - \frac{E_{11}}{E_{11f}}\upsilon_{f21}\right)\tilde{\sigma}_{22}\right] = 1\,;\ \tilde{\sigma}_{11} \geq 0 \\
f_{E,FF,C} &= \frac{1}{X_C}\left[\tilde{\sigma}_{11} - \left(\upsilon_{21} - \frac{E_{11}}{E_{11f}}\upsilon_{f21} m_{\sigma f}\right)\tilde{\sigma}_{22}\right] = 1\,;\ \tilde{\sigma}_{11} < 0 \\
f_{E,IFF,T} &= \sqrt{\left(\frac{\tilde{\sigma}_{21}}{S_{21}}\right)^2 + \left(1 - p^{+}_{\upsilon p}\frac{Y_T}{S_{21}}\right)^2\left(\frac{\tilde{\sigma}_{22}}{Y_T}\right)^2} + p^{+}_{\upsilon p}\frac{\tilde{\sigma}_{22}}{S_{21}} = 1\,;\ \tilde{\sigma}_{22} \geq 0 \\
f_{E,IFF,C} &= \frac{1}{S_{21}}\left(\sqrt{\tilde{\sigma}_{21}^2 + \left(p^{-}_{\upsilon p}\tilde{\sigma}_{22}\right)^2} + p^{-}_{\upsilon p}\tilde{\sigma}_{22}\right) = 1\,;\ \tilde{\sigma}_{22} < 0 \\
f_{E,IFF,C} &= \left[\left(\frac{\tilde{\sigma}_{21}}{2\left(1 + p^{-}_{\upsilon\upsilon}\right)S_{21}}\right)^2 + \left(\frac{\tilde{\sigma}_{22}}{Y_C}\right)^2\right]\frac{Y_C}{\left(-\tilde{\sigma}_{22}\right)} = 1\,;\ \tilde{\sigma}_{22} < 0
\end{aligned} \tag{2}$$

In Eq. (2),E_{11}, E_{22}, G_{21} show the in-plane elastic constants,$X_{T,C}, Y_{T,C}, S_{21}$ represent the strengths in the fiber direction, transverse direction, and in-plane shear for UD Ply. Once the mesodamage is initiated by reaching the damage threshold of the material to the external load, these are accumulated with Eq. (3).

$$\begin{aligned}
d_1^j &= 1 - \frac{1}{f_{E,FF,j}}\exp\left[A_1^j\left(1 - f_{E,FF,j}\right)\right]\ ,\ A_1^j = \frac{2L_c(X_j)^2}{2E_{11}\mathcal{G}_{11}^j - L_c(X_j)^2}\ ;\ j = T, C \\
d_2^j &= 1 - \frac{1}{f_{E,IFF,j}}\exp\left[A_2^j\left(1 - f_{E,IFF,j}\right)\right]\ ,\ A_2^j = \frac{2L_c(Y_j)^2}{2E_{22}\mathcal{G}_{22}^j - L_c(Y_j)^2}\ ;\ j = T, C \\
d_{21} &= 1 - \frac{1}{f_{E,IFF,j}}\exp\left[A_{21}\left(1 - f_{E,IFF,j}\right)\right]\ ,\ A^{21} = \frac{2L_c(S_{21})^2}{2G_{21}\mathcal{G}^{21} - L_c(S_{21})^2}\ ;\ j = T, C
\end{aligned} \tag{3}$$

$\mathcal{G}_{11}^{T,C}$, $\mathcal{G}_{22}^{T,C}$, $\mathcal{G}_{21}$denote the energy release rates, and L_c is called characteristic element length, it depends on the mesh size. The one parameter plastic potential used is formularized in Eq. (4) [46].

$$f\left(\tilde{\sigma}, \tilde{p}\right) = \sqrt{\frac{3}{2}\left(\tilde{\sigma}_{22}^2 + 2a\tilde{\sigma}_{12}^2\right)} - \bar{\sigma}_y\left(\tilde{p}\right) = 0 \tag{4}$$

Where$\bar{\sigma}_y\left(\tilde{p}\right)$is the yield limit which evolves with load as a function of the accumulated equivalent plastic strain$(\tilde{p})\bar{\sigma}_y\left(\tilde{p}\right) = \beta(\tilde{p})^{\alpha}$, α, β are the hardening law exponent and coefficient, respectively. The parameter that establishes coupling between the transverse plasticity and in-plane shear plasticity is denoted with (a). This coupling parameter is found experimentally by changing the load orientations to the fiber direction by establishing a bi-axial state of stress (a combination of σ_{22} and σ_{12}) in the specimen [46]. Alternatively, Arcan fixture can be used because it has the capability to change the angle of loads for establishing a required load ratio of bi-axial state of stress. The above elasto-plastic damage model was implemented in ABAQUS/Standard through UMAT subroutine using the classical return mapping algorithm (RMA) for finding the plastic multiplicator for each increment in strain-driven mode.

3. Results and discussion

3.1. UD elastic constants

The relevant standard for tension tests in fiber direction and transverse direction of FRPs is ASTM D3039/D. The elastic constants and strengths determined in fiber direction, transverse direction, and shear stress are summarized in Table 2. The shear characterization using the two different approaches of modified Arcan fixture and through the tension test of $[\pm 45^{\circ}]_{2s}$ is discussed in the upcoming section.

3.2. Shear characterization

The in-plane shear stress-strain curve is displayed in Fig. 4-a, where a higher degree of non-linearity can be noticed. This is the typical response of most of the continuous FRPs under the shear loading. The endpoint in this shear stress-strain curve does not correspond to the ultimate failure point of the specimen because all specimens ruptured well beyond the shear strain. The actual rupture shear strain recorded was 16%, as acquired with the help of DIC shown in Fig. 4-b in comparison with the fractured specimen. The ultimate shear stress measured was 77.71 MPa at complete rupture. The higher magnitude of shear strain is associated with the fiber rotation which is also known as scissoring effect. This is the reason that failure strength in shear is selected at a 5% cut-off strain according to ASTM D3518-21 shown by the dotted line in Fig. 4-a.

In Fig. 4-c the shear performance curves obtained from the two different Arcan samples, viz. $[90^{\circ}]_{16}$ and $[0/90^{\circ}]_{4s}$, are compared with the tension test of $[\pm 45^{\circ}]_{2s}$. The recorded failure shear strengths were 45.67 MPa, 47.72 MPa, and 49.26 MPa for

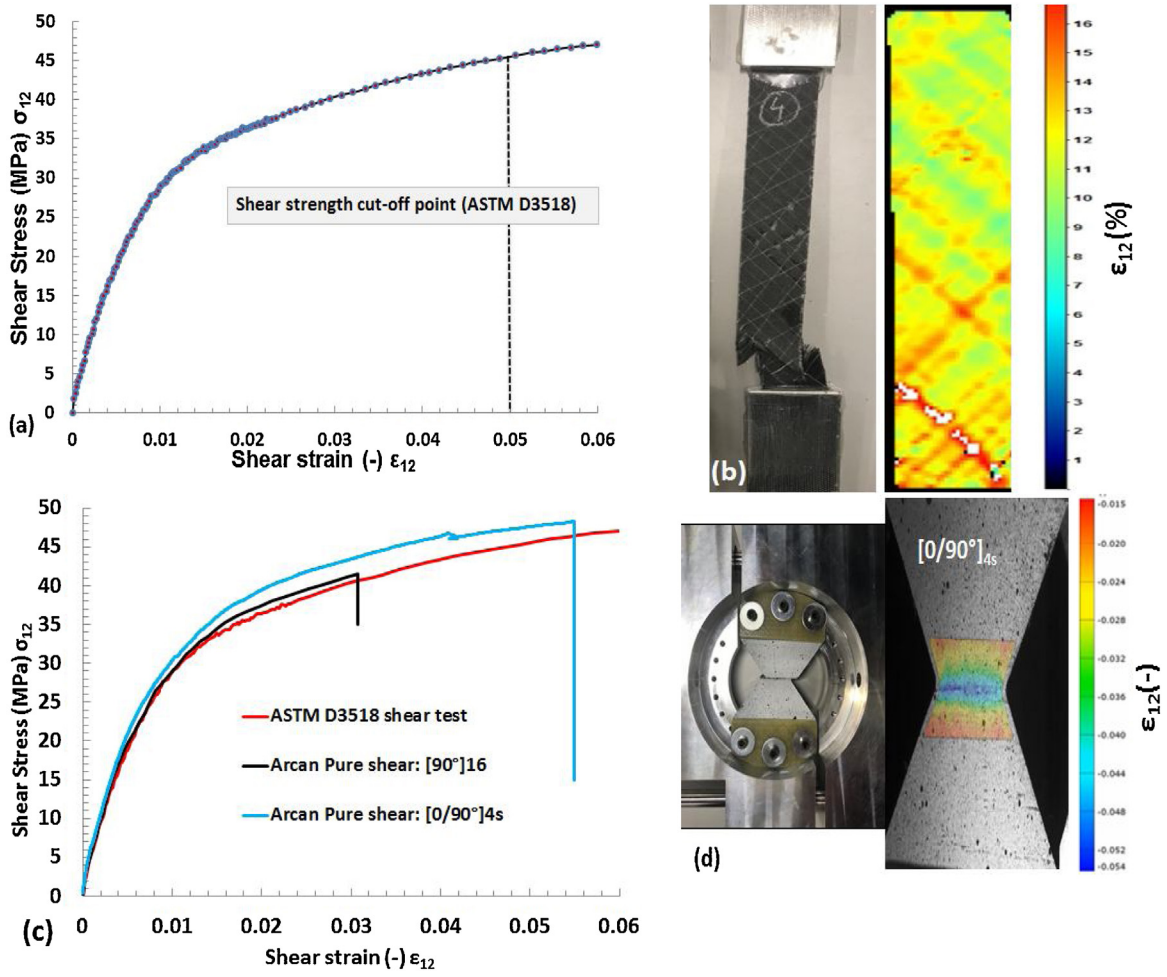

Fig. 4 – (a) In-plane shear-stress strain plot of $[\pm 45^\circ]_{2s}$ specimen, (b) DIC ultimate shear strain and one of fractured specimens (c) shear stress-strain comparison with Arcan fixture (d) DIC ultimate shear strain field and one of the fractured specimens of Arcan test.

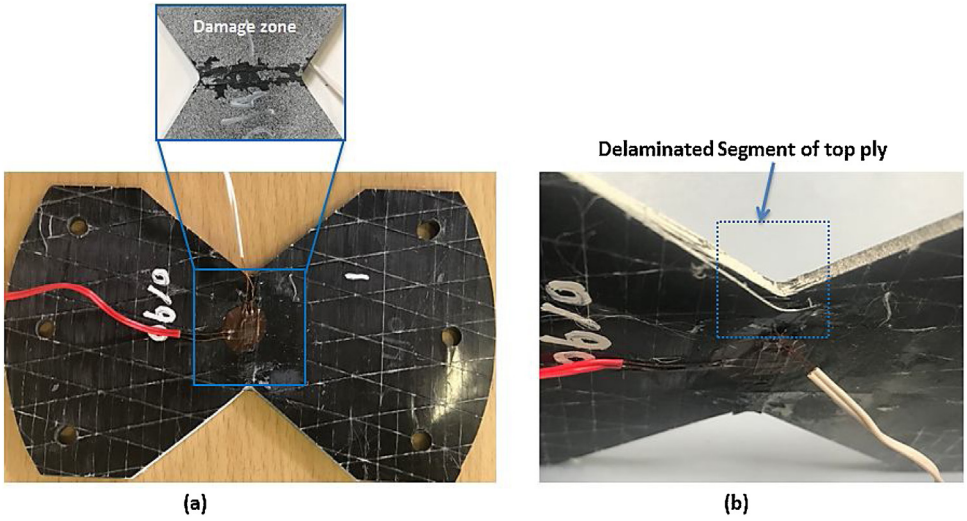

Fig. 5 – $[0/90^\circ]_{4s}$ pure shear post-test Arcan sample (a) damage zone, (b) macroscopic delamination.

Table 2 – Elastic constants.

E_{11} (GPa)	E_{22} (MPa)	G_{21} (MPa)	υ_{12}	X_T (MPa)	Y_T (MPa)	S_{21} (MPa)
115.0 ± 1.1	9.8 ± 0.9	4.05 ± 0.8	0.31	1950.0 ± 90	43.2 ± 4.0	45.67 ± 2.1

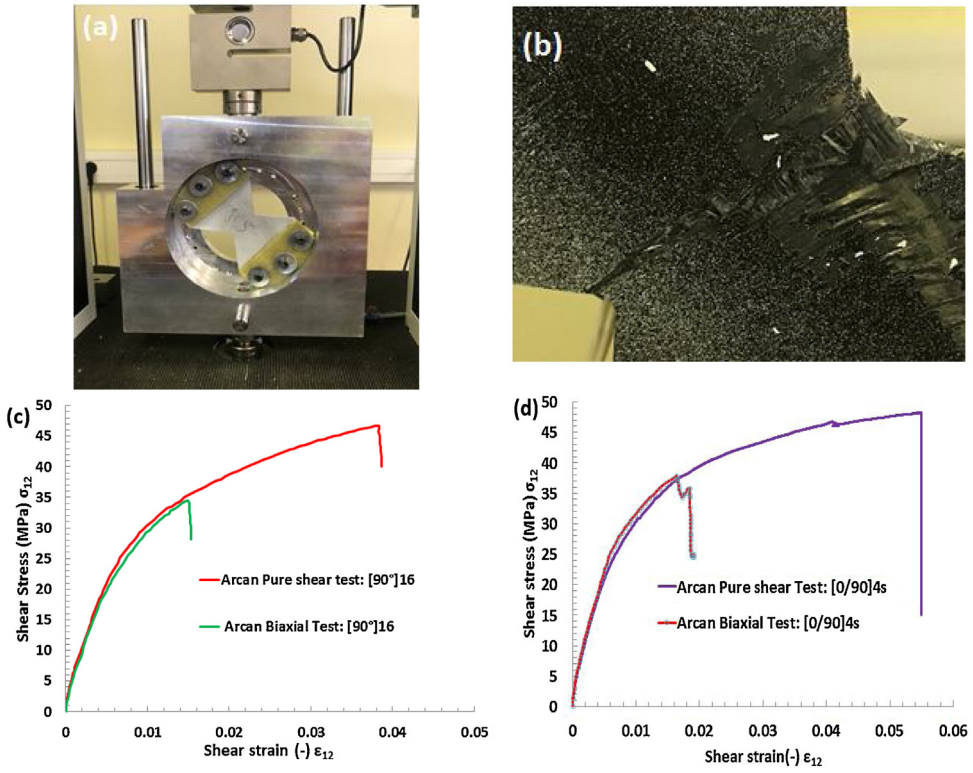

Fig. 6 – (a) Bi-axial stress test set-up, (b) One of the fractured specimens, (c) $[90°]_{16}$ laminates bi-axial response (d) $[0/90°]_{4s}$ bi-axial test result.

the tension test of $[\pm45°]_{2s}$, Arcan tests of $[90°]_{16}$, and $[0/90°]_{4s}$, respectively. It has been reported by El-Hajjar et al. [14] that a shear test based on the Arcan fixture presents higher shear behavior than a UD tension test of $[\pm45°]_{2s}$ due to the existence of normal stress components in the later. An Arcan specimen of $[90°]_{16}$ failed at 3.8% shear strain while the cross-ply $[0/90°]_{4s}$ failed at 5.4% shear strain, approximately. The higher failure strain in case of $[0/90°]_{4s}$ is attributed to the fiber rotation in contrast to the UD laminate $[90°]_{16}$. In the $[90°]_{16}$ pure shear test, the stress continuously increased until a peak value and then final rupture occurred. One of the fractured specimens of the pure shear test of $[0/90°]_{4s}$ are shown in Fig. 4-d in addition to the shear strain field distribution obtained through DIC. The uniformity in the shear strain field is clear in the vicinity of the notch section and the failure shear strain recorded was -5.4%. It can be noticed that cracks run parallel to the notch-to-notch direction, and the damage is limited to the notch area which is desired to avoid pre-mature failure at the holes for clamping the specimen with the fixture. Moreover, a drop in the stress was observed in the $[0/90°]_{4s}$ pure shear test at a value of 46.20 MPa (Fig. 4-c), which is associated with delamination. The damage zone and the macroscopic delamination in the top ply of the cross-ply $[0/90°]_{4s}$ Arcan specimen are shown in Fig. 5.

3.3. *Bi-axial loading*

In case of bi-axial loading, combined loading of shear and normal tensile stress was applied indirectly by rotating specimens in the Arcan fixture. First $[90°]_{16}$ laminate was tested at 45° in the Arcan fixture, as shown in Fig. 6-a, where the ratio between normal stress and shear stress is one. The fractured specimen and the shear response are given in Fig. 6-b, and Fig. 6-c, respectively. It is clear that at the bi-axial condition the specimen failed at a lower ultimate shear strength, which has similarly been reported in [14,17], due to the existence of the normal stress components which also contributed to failure. The ultimate failure shear stress obtained in the bi-axial stress state was 34.55 MPa at 1.4% shear strain, compared to the pure shear test where it was recorded at 47.72 MPa. Hence, transverse stress degraded the shear strength by a decrease of 27.5%. In the same manner, $[0/90°]_{4s}$ specimens were tested in a bi-axial stress case as depicted in Fig. 6-d. The failure shear stress obtained in the bi-axial experiment was 37.31 MPa at a shear strain of 1.56%, which is inferior to the pure shear test of a similar specimen i.e. 49.26 MPa. Accordingly, a 24.26% decrease is reported in this test associated with the collaborative effect of combined loading.

3.4. *Two-steps loading experiments*

The two-step loading on $[0/90^\circ]_{4s}$ specimens were completed to investigate the effects of diffused damage induced in pure shear step on the tensile behavior of the laminate. Firstly, the cross ply laminate was loaded in pure shear conditions in an Arcan fixture up to predefined loads less than the ultimate shear strength. The pre-defined load values were about 75% (3 K N), and 65 % (2.5 K N) of the shear failure loads measured in Fig. 4-c for $[0/90^\circ]_{4s}$ specimens in Arcan tests. The mentioned load levels were chosen from the shear stress-strain plot of tests according to ASTM D3518-21 in Fig. 4-a where non-linearity is captured showing the onset of diffused damage in the matrix material. Diffused damage includes fiber/matrix de-bonding and matrix micro-cracks. These load magnitudes are sufficient to trigger the diffused damage in the matrix material which is usually less strong. Moreover, the threshold of transverse meso-cracking of the material analyzed in the present work is greater than the load levels which is required to induce only the diffused damage in the Arcan specimens in the first step. In the second load-step, the same specimens were unmounted and rotated at an angle of 90° in the fixture to apply tension load. The tensile behavior of specimens with prior damage in shear load-step was compared with the monotonic tensile stress-strain responses of the pristine Arcan samples tested in single tension step.

The shear stress-strain profiles of the two specimens, which were unloaded at 2.5 K N and 3 K N in pure shear stress conditions in Arcan fixture, are shown in Fig. 7-a. Test curve of one-step monotonic shear test of $[0/90^\circ]_{4s}$ has also been plotted. It appears that the shear stress-strain profiles applied in the first step followed each other closely in addition to the monotonic pure shear test curve of $[0/90^\circ]_{4s}$. In the second step, the specimens were unmounted and examined carefully to observe any macro-damage or failure at the bolted holes. No macro-damage was determined and the bolted holes were also found intact. It is suggested that proper inspection of transverse matrix cracking and diffused damage at this unloading stage should be undertaken by employing non-destructive techniques. The specimens were then clamped again in the Arcan fixture at $\theta = 90^\circ$. Tensile load at a rate of 2 mm/min was applied until the specimens ruptured. The tensile mechanical behavior of these two pre-damaged specimens in the first shear loading step in addition to the specimen with no initial damage designated as a pristine sample, are compared in Fig. 7-b.

Fig. 7-b demonstrates that diffused damage in shear influenced the response of the Arcan specimen in tension. The percent decrease in the maximum breaking strength of the laminate in tension for the sample unloaded at 3 K N was 17.5 %. On the other hand, a percent decrease of 12% in the tensile breaking strength was recorded for the sample which was unloaded in shear test at a lower value of 2.5 K N. As expected that higher unloading load level accumulated more damage in the first sample thus causing more degradation in the laminate strength. It is well-recognized in the literature that the dominant diffused failure mechanisms are fiber/matrix debonding and matrix micro-cracking when FRPs are loaded in shear stress. As a consequence, the degradation given in

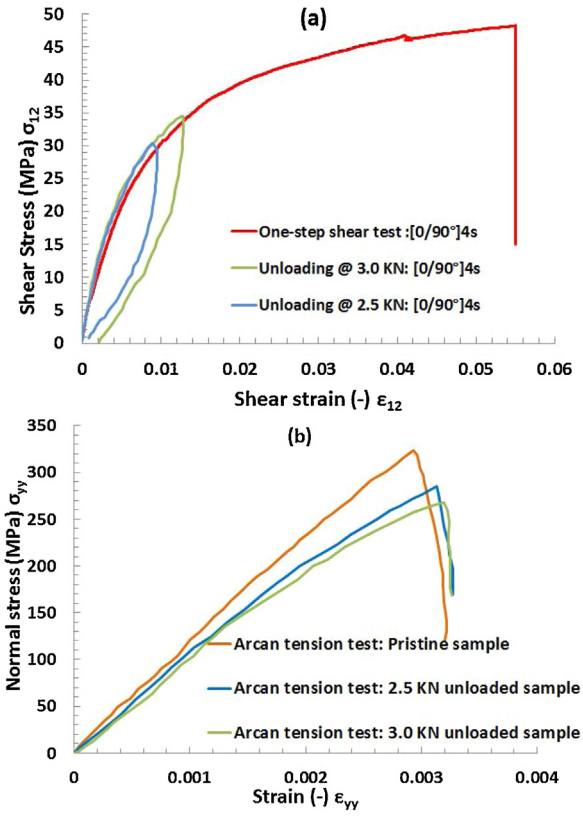

Fig. 7 – (a) $[0/90^\circ]_{4s}$ specimens in pure shear stress state, (b) $[0/90^\circ]_{4s}$ specimens in tension load.

Fig. 7-b is attributed to diffused damage induced in the first load-step. These failures degraded shear and transverse elastic properties of the laminate. Fiber direction elastic constants are less affected by failure in shear load, but as this laminate was cross-ply, the 90° ply contributed less in carrying the load. Hence, the 90° pre-damaged plies caused this difference. In contrast, ply aligned to the load in the second step of tensile load in the Arcan fixture can be expected to carry the same load because the failure mechanisms of the first shear step are not very influential on the fiber response.

4. Numerical simulations

The pure shear case of cross-ply $[0/90^\circ]_{4s}$ Arcan experiments was simulated using a 2D elasto-plastic model developed by the authors of the present work [22]. Due to shear behavior in FRPs being highly non-linear, an elasto-plastic model is necessary to predict the accurate state of stress. Once the state of stress is reliable, then damage can be accurately predicted. This model was accordingly implemented in ABAQUS via UMAT, where the right side set of holes were fixed by defining the fixed displacement boundary conditions (BCs) on the three reference points which were linked with the circumferential nodes on the holes by specifying beam constraints. For the application of shear load, three reference points were defined like for the BCs, and then displacement load was applied on these reference points in y-axis. The boundary conditions and load points, as well as meshing, are further

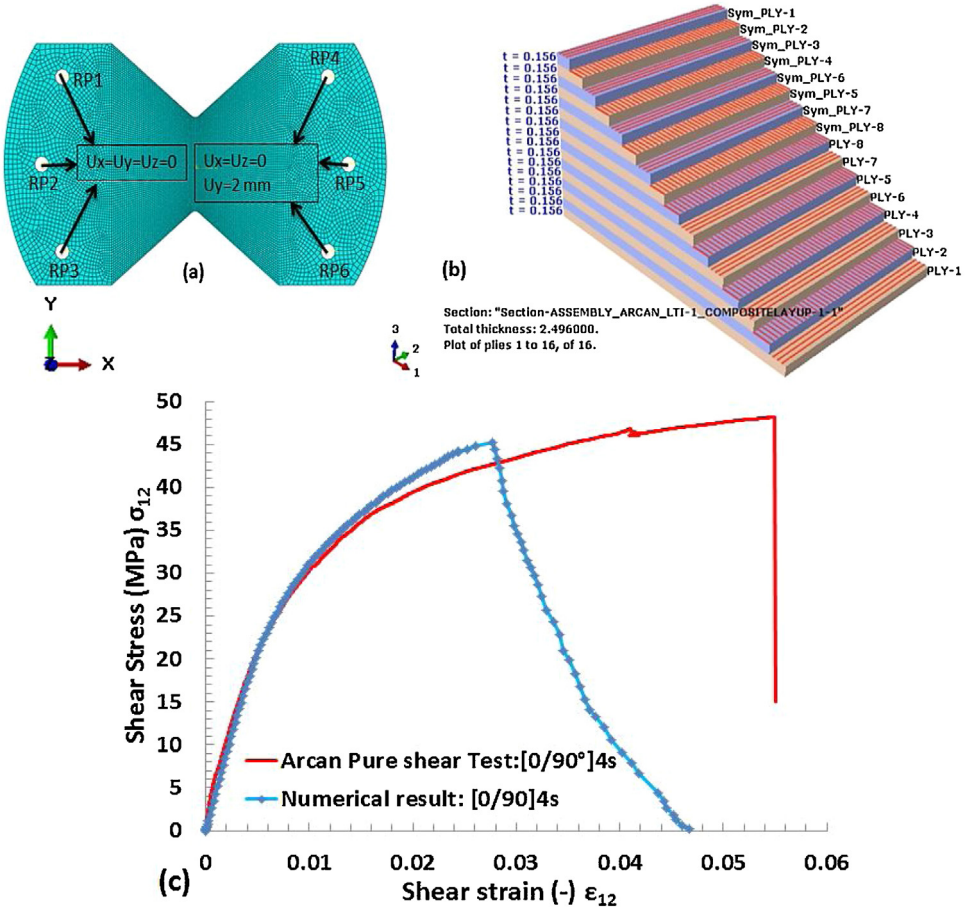

Fig. 8 – $[0/90^\circ]_{4s}$ shear simulation set-up, (a) meshing and BCs, (b) stacking sequence, (c) numerical prediction for $[0/90^\circ]_{4s}$ in pure shear.

explained in Fig. 8-a. A 4-node plane stress element with reduced integration formulation (SR4) was used during meshing.

The shear strain was calculated as the average of the shear strains at the centroids of the elements bounded by the area equal to the size of the strain gauge used in the experiments. For this purpose, element sets were defined in ABAQUS. The shear stress was calculated by dividing the sum of the reaction forces in the y-axis at the three reference points (RP4, RP5, RP6) with the sectional area of the notch section. The numerical prediction of the developed model in [22] and the pure shear experiment of $[0/90^\circ]_{4s}$ are contrasted in Fig. 8-c. The predicted failure shear strength is 45.2 MPa, less than the ultimate failure strength in the Arcan experimental value of 49.26 MPa. This is due to the fact that the model uses shear strength obtained from the in-plane tension test of $[\pm 45^\circ]_{2s}$, reported as lower than the Arcan pure shear test. The shear strain field obtained based on the numerical simulation at failure is compared with DIC given in Fig. 9. The model underestimated failure shear strain with an error of 14% which is attributed to the provision of the lower shear strength to the model based on ASTM D3518-21 rather than the Arcan based measured shear strength. It was noted in the FEM simulations of cross-ply Arcan specimen that the shear strain distribution was similar in magnitude in 0° and 90° plies, but was opposite in direction which complies with classical laminate theory (CLT).

As the elasto-plastic model used in the present simulations is based on 2D Puck's theory for triggering mesoscale damage, the Mode-A failure mode was detected in the plies because the condition for this mode is that $\tilde{\sigma}_{22} \geq 0$ [5]. The damage initiation and subsequent progression in ply 2 are shown in Fig. 10. A maximum value of 0.99 was kept for the damage during all simulations to avoid numerical singularity. Based on the FEM results it can be concluded that an identical state of stress field was obtained in all the plies. Therefore, damage initiation and accumulation were also similar in all the plies. Fig. 11 describes the damage predicted with the numerical simulation in reference to the experimental fractured specimen of $[0/90^\circ]_{4s}$.

5. Conclusions

In this study, the robustness of Arcan fixture was demonstrated to investigate the impact of diffused damage on the transverse matrix cracking and on the global response of the cross ply laminate. Arcan fixture can be easily used by testing the same specimens at a variety of different angles and load ratios of interest between the shear stress and normal

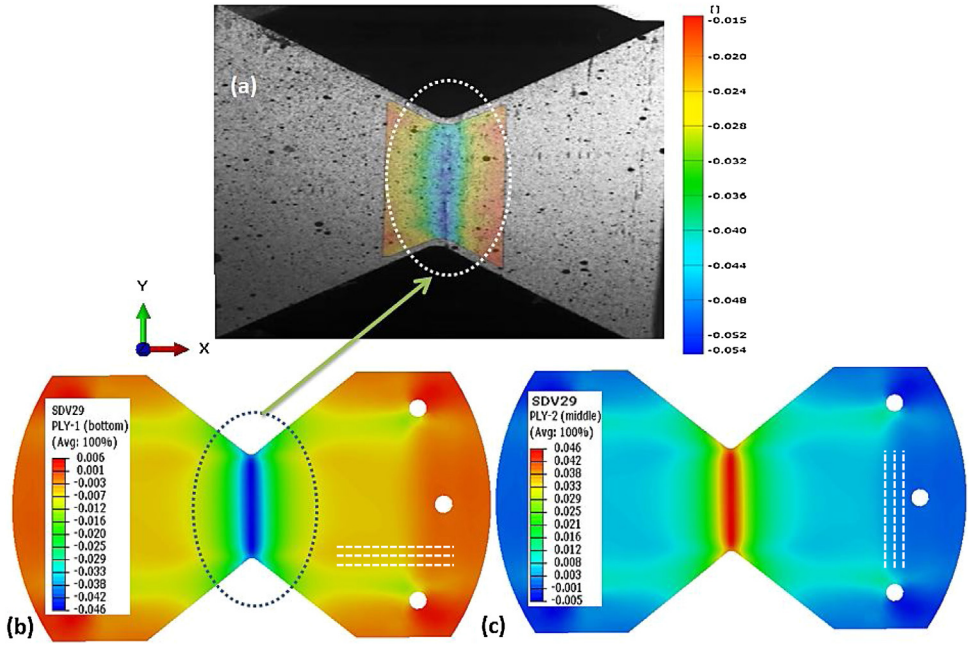

Fig. 9 – $[0/90^{\circ}]_{4s}$ shear strain contour at failure (a) the top ply of Arcan specimen recorded by DIC, (b) FEM based shear strain field at the top ply (fiber along y-direction shown by dotted lines) (c) shear strain field in ply 2 (fiber along the x-direction shown by dotted lines).

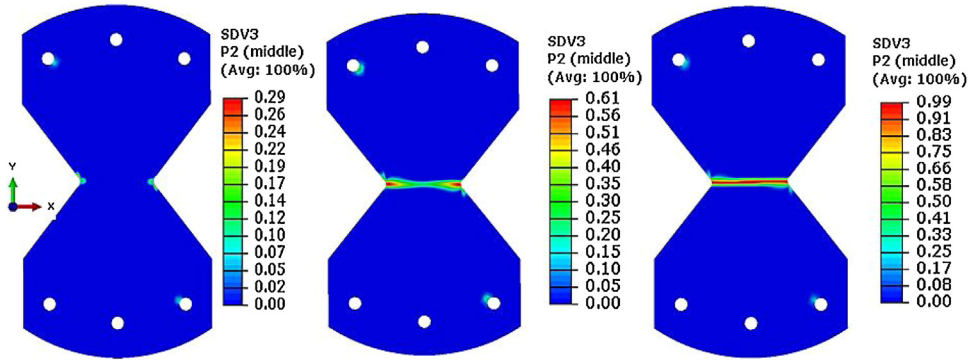

Fig. 10 – Puck mode-A damage initiation and saturation: (SDV3=damage state variable in shear stress).

stress. Uni-directional (UD) characterization was performed and the elastic properties were used in the numerical simulations. Several butterfly specimens of $[90^{\circ}]_{16}$ and $[0/90^{\circ}]_{4s}$ were manufactured and tested in pure shear and bi-axial loading. A decrease of 27.5% was recorded in the shear strength by rotating the Arcan specimen to 45°. The shear mechanical behaviors were characterized and compared by two different test set-ups. The realistic shear response of FRPs can be measured experimentally using Arcan fixture than the ASTM D3518-21 because of no stress interaction in the Arcan test.

While highlighting the effects of diffused damage on the laminate tensile response, two steps loading of shear and tensile modes were applied with the help of Arcan fixture by rotating the same specimens from the state of pure shear to the state of normal stress. The unloaded load levels were selected in such a way that these were greater than the thresholds of the diffused damage and yet less than the meso-damage onset limit. Accordingly, these values were chosen from the shear test where non-linearity first appeared during the test. A percent decrease of 17.5% in the maximum breaking strength of the laminate in tension was measured for the sample unloaded at 3 KN. The other sample, which was unloaded at a lower load level, resulted into less percent decrease of 12% as expected in the tensile breaking strength.

The Arcan test of pure shear case was also supplemented with numerical simulations using the elastoplastic damage coupled constitutive law assuming a plane stress case. It is necessary to use the non-linear material models to accurately capture the typical higher non-linear behavior of FRPs in case of shear stress. ABAQUS UMAT was used for the implementation. The shear strain field at failure based on the numerical simulation is in good correspondence qualitatively with the

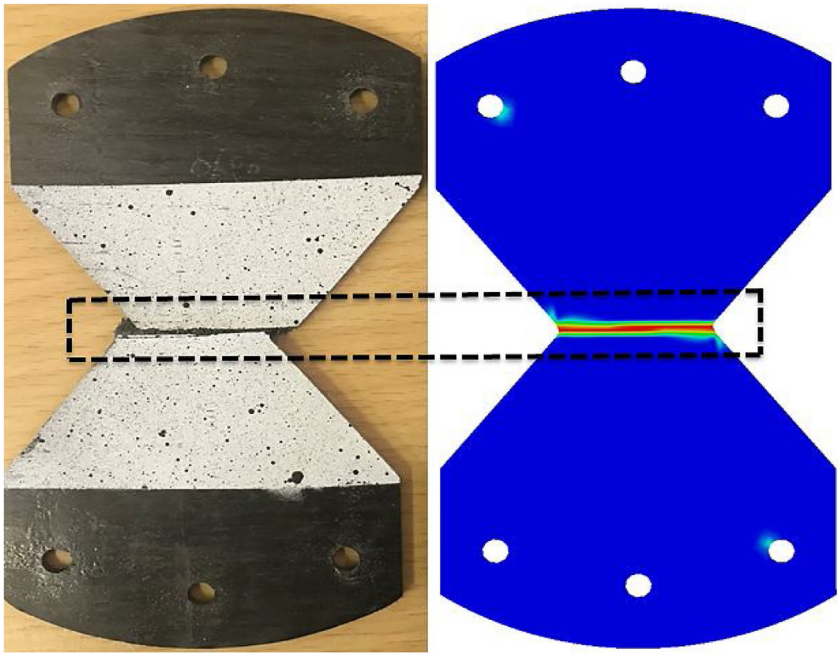

Fig. 11 – Fractured specimen and damage contour (Mode-A, Puck's theory).

shear strain field acquired via digital image correlaion (DIC). Nevertheless, the failure strain is underestimated with 14% error by the developed model.

It is suggested that an extensive testing campaign is required to further study diffused damage transformation into transverse cracking to exploit Arcan fixture versatility in terms of load orientations. Moreover, non-destructive techniques should be used to detect and quantify diffuse damage and subsequent coalescence into mesoscale transverse cracking.

Conflicts of interest

The authors declare no conflicts of interest.

Acknowledgements

This work was partially supported by The China National Key R&D Program (No. 2018YFB0803600), Natural Science Foundation of China (No. 61801008), Beijing Natural Science Foundation National (No. L172049), Scientific Research Common Program of Beijing Municipal Education Commission (No. KM201910005025).

The first author (Israr Ud Din) is extremely grateful to Higher Education Commission (HEC), Pakistan and Campus France for the provision of financial support to his doctoral studies based in France. Pei Hao acknowledges the financial support provided by China Scholarship Council (CSC). The authors also like to acknowledge Dr. Dymtro Vasiukov, IMT Lille Douai (France) for his assistance in acquiring the strain fields with the help of digital image correlation.

REFERENCES

[1] Aamir M, Tolouei-Rad M, Giasin K, Nosrati A. Recent advances in drilling of carbon fiber–reinforced polymers for aerospace applications: a review. Int J Adv Manuf Technol 2019;105:2289–308.

[2] Ud Din I, Naresh K, Umer R, Khan KA, Drzal LT, Haq M, et al. Processing and out-of-plane properties of composites with embedded graphene paper for EMI shielding applications. Compos Part A Appl Sci Manuf 2020;134:105901.

[3] Shah SZH, Karuppanan S, Megat-Yusoff PSM, Sajid Z. Impact resistance and damage tolerance of fiber reinforced composites: a review. Compos Struct 2019;217:100–21.

[4] Olsson R. A survey of test methods for multiaxial and out-of-plane strength of composite laminates. Compos Sci Technol 2011;71:773–83.

[5] Puck A, Schurmann H. Failure analysis of FRP laminates by means of physically based phenomenological models. Composite Science and Technology 2002;62:1633–62.

[6] Cuntze RG. Efficient 3D and 2D failure conditions for UD laminae and their application within the verification of the laminate design. Compos Sci Technol 2006;66:1081–96.

[7] Ud Din I, Panier S, Hao P, Franz G, Bijwe J, Hui L. Finite element modeling of indentation and adhesive wear in sliding of carbon fiber reinforced thermoplastic polymer against metallic counterpart. Tribol Int 2019;135:200–12.

[8] Van Paepegem W, De Baere I, Degrieck J. Modelling the nonlinear shear stress–strain response of glass fibre-reinforced composites. Part I: experimental results. Compos Sci Technol 2006;66:1455–64.

[9] Tan WF, Brian G. Modelling the nonlinear behaviour and fracture process of AS4/PEKK thermoplastic composite under shear loading. Compos Sci Technol 2016;126:60–77.

[10] Khashaba UA. In-plane shear properties of cross-ply composite laminates with different off-axis angles. Compos Struct 2004;65:167–77.

[11] Almeida JHS, Angrizani CC, Botelho EC, Amico SC. Effect of fiber orientation on the shear behavior of glass fiber/epoxy composites. Mater Des 2015;65:789–95.
[12] Arcan M, Hashin Z, Voloshin A. A method to produce uniform plane-stress states with applications to fiber-reinforced materials. Exp Mech 1977:141–6.
[13] Smits LS. Design of a cylindrical specimen for biaxial testing of composite materials. J Reinf Plast Compos 1997;16:550–64.
[14] El-Hajjar RH-A, Rami. In-plane shear testing of thick-section pultruded FRP composites using a modified Arcan fixture. Compos Part B Eng 2004;35:421–8.
[15] Alfonso L, Uguen A, Badulescu C, Cognard JY, Bonnemains T, Lolive E, et al. Determination of the 3D failure envelope of a composite based on a modified Arcan test device. Compos Struct 2015;131:585–93.
[16] Cognard JY, Sohier L, Davies P. A modified Arcan test to analyze the behavior of composites and their assemblies under out-of-plane loadings. Compos Part A Appl Sci Manuf 2011;42:111–21.
[17] Gning PB, Delsart D, Mortier JM, Coutellier D. Through-thickness strength measurements using Arcan's method. Compos Part B Eng 2010;41:308–16.
[18] Sawadogo H, Panier S, Hariri S. Experimental and numerical study of the fatigue of GFRP composites under complex loadings. Japan: ICMFF10; 2013.
[19] Smits A, Van Hemelrijck D, Philippidis TP, Cardon A. Design of a cruciform specimen for biaxial testing of fibre reinforced composite laminates. Compos Sci Technol 2006;66:964–75.
[20] Li Y, Zhang K, Zhang B. Shear fatigue test and life prediction of composite laminates trans tech publications, Switzerland; 2003.
[21] Nouri H, Lubineau G, Traudes D. An experimental investigation of the effect of shear-induced diffuse damage on transverse cracking in carbon-fiber reinforced laminates. Compos Struct 2013;106:529–36.
[22] Ud Din I, Hao P, Franz G, Panier S. Elastoplastic CDM model based on Puck's theory for the prediction of mechanical behavior of Fiber reinforced Polymer (FRP) composites. Compos Struct 2018;201:291–302.
[23] Yen S, Craddock J, Teh K. Evaluation of a modified Arcan fixture for the in-plane shear test of materials. Exp Tech Urol Nephrol 1998;12:22–7.
[24] Tan JLY, Deshpande VS, Fleck NA. Failure mechanisms of a notched CFRP laminate under multi-axial loading. Compos Part A Appl Sci Manuf 2015;77:56–66.
[25] Ud Din I, Hao P, Panier S, AKhan K, Aamir M, Gerald F, et al. Design of a new Arcan fixture for in-plane pure shear and combined normal/shear stress characterization of fiber reinforced polymer composites. Exp Tech 2020;44:231–40.
[26] Hao P, Ud Din I, Panier S. Development of Modified Arcan Fixture for biaxial loading response of fiber-reinforced composites. Polym Test 2019;80:106148.
[27] Ladevèze P, Le Dantec E. Damage modelling of the elementary ply for laminated composites. Compos Sci Technol 1992;43:257–67.
[28] Maimí P, Camanho PP, Mayugo JA, Dávila CG. A continuum damage model for composite laminates: part I – constitutive model. Mech Mater 2007;39:897–908.
[29] Chen JF, Morozov EV, Shankar K. A combined elastoplastic damage model for progressive failure analysis of composite materials and structures. Compos Struct 2012;94:3478–89.
[30] Vasiukov D, Panier S, Hachemi A. Non-linear material modeling of fiber-reinforced polymers based on coupled viscoelasticity–viscoplasticity with anisotropic continuous damage mechanics. Compos Struct 2015;132:527–35.
[31] Ribeiro ML, Tita V, Vandepitte D. A new damage model for composite laminates. Compos Struct 2012;94:635–42.
[32] Völkerink O, Petersen E, Koord J, Hühne C. A pragmatic approach for a 3D material model considering elasto-plastic behaviour, damage initiation by Puck or Cuntze and progressive failure of fibre-reinforced plastics. Comput Struct 2020;236:106280.
[33] Boutaous A, Peseux B, Gornet L, Bélaidi A. A new modeling of plasticity coupled with the damage and identification for carbon fibre composite laminates. Compos Struct 2006;74:1–9.
[34] Arabatti T, Parambil NK, Gururaja S. Micromechanical modeling of damage development in polymer composites. Advanced Composites Letters 2016;25:56–62.
[35] Lubineau G, Ladevèze P. Construction of a micromechanics-based intralaminar mesomodel, and illustrations in ABAQUS/Standard. Comput Mater Sci 2008;43:137–45.
[36] Xia Z, Chen Y, Ellyin F. A meso/micro-mechanical model for damage progression in glass-fiber/epoxy cross-ply laminates by finite-element analysis. Composites Science and Technolgy 2000;60:1171–9.
[37] Xavier A. New advances in damage mechanics and computational methods for composites: from research to industry for spatial applications. Composite Science and Technology 2001;61:2337–44.
[38] Ulrich M, Robin T, Roland H. Laminate damage model for composite structures. Compos Struct 2015;136:441–9.
[39] Forghani A, Zobeiry N, Poursartip A, Vaziri R. A structural modelling framework for prediction of damage development and failure of composite laminates. Journal of Compoiste Materials 2013;47:2553–73.
[40] He G, Liu Y, Hammi Y, Bammann DJ, Horstemeyer MF. A combined viscoelasticity-viscoplasticity-anisotropic damage model with evolving internal state variables applied to fiber reinforced polymer composites. Mech Adv Mater Struct 2020.
[41] He G, Liu Y, Deng X, Fan L. Constitutive modeling of viscoelastic–viscoplastic behavior of short fiber reinforced polymers coupled with anisotropic damage and moisture effects. Acta Mech Sin 2018;35:495–506.
[42] He G, Liu Y, Bammann DJ, Francis DK, Chandler MQ, Horstemeyer MF. A multiphase internal state variable model with rate equations for predicting elastothermoviscoplasticity and damage of fiber-reinforced polymer composites. Acta Mech 2019;230:1745–80.
[43] He G, Liu Y, Bammann DJ, Horstemeyer MF. An elastothermoviscoplasticity anisotropic damage model for short Fiber reinforced polymer composites. International mechanical engineering congress and exposition IMECE2018. Pittsburgh, PA, USA; 2018.
[44] Kachanov LM. Time of the rupture process under creep condition. Jzvestia Akad Nauk 1958;8:26–31.
[45] Ud Din I, Hao P, Aamir M, Franz G, Panier S. FEM implementation of the coupled Elastoplastic/Damage model: failure prediction of Fiber reinforced polymers (FRPs) composites. Journal of Solid Mechanics 2019;11:842–53.
[46] Sun CT, Chen JL. A simple flow rule for characterizing non-linear Behavior of Fiber composites. J Compos Mater 1988;23:1009–20.